Materialwiss. Werkstofftech. **2021**, *52*, 1394–1412 doi.org/10.1002/mawe.202100042

Self-lubricating CrAlVN coatings for turning of Ti6Al4V: oxidation and wear behavior

Selbstschmierende CrAlVN-Beschichtungen zum Drehen von TiAl6V4: Oxidations- und Verschleißverhalten

K. Bobzin[1], T. Brögelmann[1], N. Stachowski[1], W. Hintze[2], C. Möller[2], P. Ploog[2]

The titanium alloy Ti6Al4V enables significant performance increases in various branches of industry. Nevertheless, it is difficult to machine, because of its material properties. Due to the low thermal conductivity of titanium, the heat generated while turning Ti6Al4V mainly flows into the tool leading to high temperature loads. In addition, the comparatively low Young's modulus and high yield strength contributes to high mechanical stresses during machining. Temperature active, self-lubricating physical vapor deposition hard coatings appear to be suitable for reducing friction and tool wear during turning of Ti6Al4V compared to the most commonly used uncoated carbide tools. The ability of the coating to form lubricating oxide phases at high temperatures is crucial for this purpose. This paper investigates the oxidation and diffusion behavior of vanadium doped chromium aluminium nitride (CrAlN) coatings after heat treatment at $\vartheta = 600\,^{\circ}\mathrm{C}$, $\vartheta = 700\,^{\circ}\mathrm{C}$ und $\vartheta = 800\,^{\circ}\mathrm{C}$ in atmosphere as well as the resulting coating properties. The wear behavior of certain coating variants while turning of Ti6Al4V is analyzed.

Keywords: Physical vapor deposition / Self-lubrication / Turning / Titanium / Wear

Die Titanlegierung TiAl6V4 ermöglicht bedeutende Leistungssteigerungen in diversen Industriezweigen, ist jedoch aufgrund ihrer Werkstoffeigenschaften schwer zerspanbar. Aufgrund ihrer geringen thermischen Leitfähigkeit fließt bei der Bearbeitung die Wärme hauptsächlich in das Werkzeug, was in hohen Zerspantemperaturen resultiert. Zusätzlich führt der vergleichsweise geringe Elastizitätsmodul zu hohen mechanischen Lasten während der Zerspanung. Temperaturaktive selbstschmierende physikalische Gasphasenabscheidung Hartstoffschichten scheinen daher geeignet, die Reibung und damit den Werkzeugverschleiß der standardmäßig eingesetzten unbeschichteten Hartmetallwerkzeuge während der Drehbearbeitung von TiAl6V4 zu verringern. Die Fähigkeit der Beschichtung, schmierende Oxidphasen bei hohen Temperaturen zu bilden, ist hierfür entscheidend. Im vorliegenden Paper werden das Oxidations- und Diffusionsverhalten von Vanadium dotierten Chrom-Aluminium-Nitrid (CrAlN) Beschichtungen nach der Wärmebehandlung bei $\vartheta = 600\,^{\circ}\mathrm{C}$, $\vartheta = 700\,^{\circ}\mathrm{C}$ und $\vartheta = 800\,^{\circ}\mathrm{C}$ an Atmosphäre sowie resultierende Schichteigenschaften untersucht. Zusätzlich wird das Verschleißverhalten von ausgewählten Schichtvarianten während der Drehbearbeitung von TiAl6V4 analysiert.

[1] RWTH Aachen University, Surface Engineering Institute, Aachen, Germany
[2] Hamburg University of Technology (TUHH), Institute of Production Management and Technology, Hamburg, Germany

Corresponding author: N. Stachowski, RWTH Aachen University, Surface Engineering Institute, Kackertstraße 15, 52072, Aachen, Germany,
E-Mail: stachowski@iot.rwth-aachen.de

Schlüsselwörter: Physikalische Gasphasenabscheidung / Selbstschmierung / Drehen / Titan / Verschleiß

1 Introduction

The use of the titanium alloy Ti6Al4V enables significant performance increases in the automotive industry as well as in aerospace-, energy- and medical-technology due to the combination of a high strength with a low density. Beside others, the properties of this alloy include a heat resistance of up to approximately $\vartheta = 550$ °C, a low thermal conductivity of $\lambda = 5.8$ W/mK and a low Young's modulus of $E = 110$ Gpa–140 GPa. Because of these properties and the tendency to cause abrasive tool wear, Ti6Al4V is considered as difficult to machine [1]. In general, the low thermal conductivity leads to high temperatures at the cutting edge, because the heat cannot dissipate through the chip and into the workpiece. Furthermore, the remaining high temperature strength and the low Young's modulus of Ti6Al4V lead to self-excited vibrations and increased stress concentration in the cutting edge. In addition to these thermomechanical properties, titanium alloys have a significant tendency to form chemical reactions with other cutting materials and build-up edges [2]. As a result, high tool wear leads to increased process costs. The machining of complex components made of titanium alloys is not yet economically satisfactory. In order to reduce tool wear, a frequently used possibility is the application of hard coatings by physical vapor deposition. Aim is, that the hard coating separates the workpiece and the cemented carbide tool during the cutting process in order to reduce frictional forces and adhesion between tool and workpiece in the tribological contact [1]. A self-lubricating effect in the coating system can further decrease the friction forces. Due to process temperatures up to $\vartheta = 1{,}000$ °C, lubricating oxide phases are particularly interesting for machining of Ti6Al4V [3]. At elevated temperatures in an oxygen containing atmosphere the transition metal vanadium is able to form lubricating oxide phases with comparatively low shear strength at the surface [4]. Advantageous is, that those lubricating oxide phases are able to renew themselves continuously during application time. This is because the temperature active vanadium diffuses to the surface if the lubricating oxide layer is worn out at the tribological contact point. Many of the formed lubricating oxides can be classified into a number of sub-stoichiometric compounds, which are generally referred as Magnéli-phases. Their mechanism of action is based on the formation of slip planes due to a regular arrangement of oxygen defects [5]. The coating systems were deposited by using a hybrid technology consisting of direct current magnetron sputtering and high power pulse magnetron sputtering. Those hybrid processes combine the advantages of high pulse power magnetron sputtering, such as a dense coating morphology, a reduced line of sight, smoother surfaces and higher hardness with the high deposition rate of direct current magnetron sputtering [6]. Depending on the vanadium content, the oxidation behavior and resulting coating properties such as indentation hardness H_{IT} and indentation modulus E_{IT} were investigated. Additionally, cutting tests are carried out to determine the influence of the different temperature-active coatings on the machining process. These are carried out on a lathe, as the continuous cut during the turning process allows almost constant thermal stresses on the tool coating. The temperature in the contact zone is of particular importance, as this should be as constantly as possible above the required reaction temperature. Due to the poor thermal conductivity of the material and high cutting forces during machining, temperatures of over $\vartheta = 800$ °C are present in the contact zone.

2 Experimental details

2.1 Coating deposition

The coating processes were carried out in an industrial coating unit CC800/9 HPPMS, CemeCon AG, Würselen, Germany. The coating unit is equipped with two high power pulse magnetron sputtering cathodes and four direct current magnetron sputtering cathodes. The size of the targets is

A = 500 mm × 88 mm. The coatings were deposited using two different target configurations, *Figure 1*.

In case of the target configuration used for the deposition of chromium aluminium nitride (CrAlN) both high power pulse magnetron sputtering cathodes (HPPMS-1/HPPMS-2) were equipped with chromium based targets assembled with 20 aluminum plugs. The direct current magnetron sputtering cathode one (dcMS-1) and four (dcMS-4) were also equipped with those chromium aluminum targets. The direct current magnetron sputtering cathode two (dcMS-2) was equipped with an aluminum based target plugged with 20 chromium plugs. Direct current magnetron sputtering cathode three (dcMS-3) was not used for this process, Figure 1a. In order to deposit chromium aluminium vanadium nitride (CrAlVN) coating systems with varying vanadium content, the target configuration was slightly changed, Figure 1b. For this purpose, the targets at the direct current magnetron sputtering cathode two and three (dcMS-2/dcMS-3) were changed to pure vanadium. In addition, the target at the direct current magnetron sputtering cathode four (dcMS-4) was replaced by a vanadium based target, fitted with 20 aluminum plugs. The target material has a purity of 99.9 % for chromium, 99.5 % for aluminum and 99.9 % for vanadium. For the chromium aluminium nitride (CrAlN) coating a functional top layer was applied on a high power pulse magnetron sputtering-chromium-aluminium / chromium-aluminium-nitride (CrAl / CrAlN), *Figure 2*a.

In case of the vanadium containing coating systems the functional chromium aluminium vanadium nitride (CrAlVN) functional layer was also applied on a high power pulse magnetron sputtering chromium aluminium/chromium aluminium nitride (CrAl/CrAlN) interlayer, Figure 2b, c. To adjust the different vanadium content in the two coating systems, the power of the cathodes equipped with the pure vanadium targets were varied, *Table 1*. All coating systems were deposited in a threefold rotation.

2.2 Coating characterization methods

In order to conduct different analyses of coating properties, the coating systems were deposited on cemented carbide inserts of grade HW-K10, Kennametal Deutschland GmbH, Rosbach, Germany. The presented roughness values Rz and Ra were determined by means of a confocal laser scanning microscope VK-X 210, Keyence Corporation, Osaka, Japan. The morphology of the coating systems

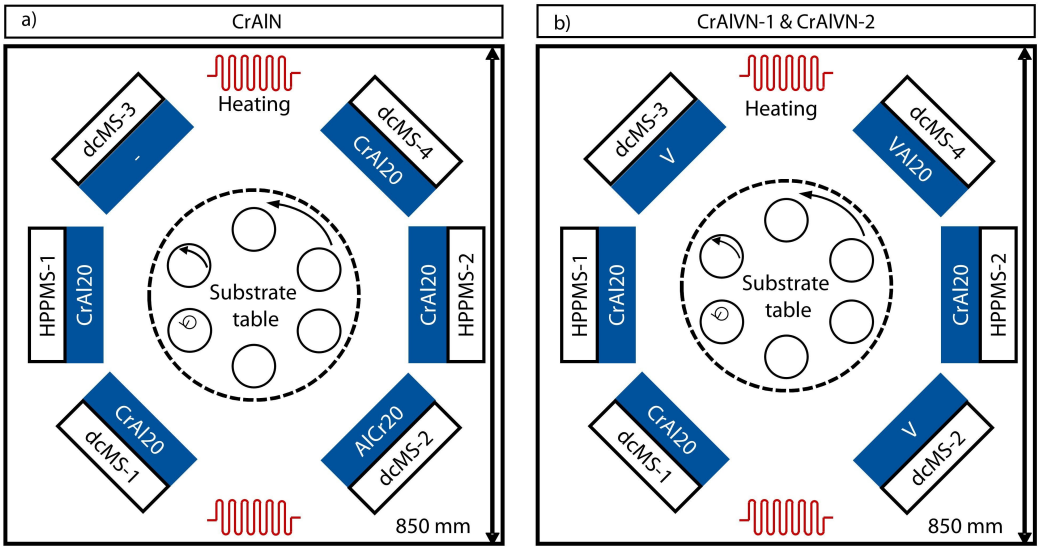

Figure 1. Schematic representation of CemeCon CC800/9 HPPMS coating unit in top view with two different target configurations for the deposition of chromium aluminum nitride (CrAlN) (a) and chromium aluminum vanadium nitride (CrAlVN) (b).

Bild 1. Schematische Darstellung der Beschichtungsanlage CemeCon CC800/9 HPPMS in der Draufsicht mit zwei unterschiedlichen Targetkonfigurationen für die Abscheidung von Chrom-Aluminium-Nitrid (CrAlN) (a) und Chrom-Aluminium-Vanadium-Nitrid (CrAlVN) (b).

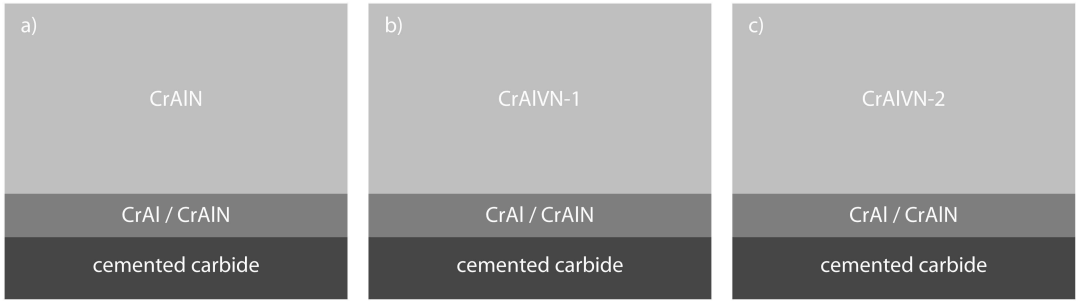

Figure 2. Schematic representation of the coating architecture of chromium aluminum nitride (CrAlN) (a), chromium aluminium vanadium nitride 1 (CrAlVN-1) (b) and chromium aluminium vanadium nitride 2 (CrAlVN-2) (c).

Bild 2. Schematische Darstellung der Schichtarchitektur von Chrom-Aluminium-Nitrid (CrAlN) (a), Chrom-Aluminium-Vanadium-Nitrid 1 (CrAlVN-1) (b) und Chrom-Aluminium-Vanadium-Nitrid 2 (CrAlVN-2) (c).

Table 1. Process parameters for coating deposition.

Tabelle 1. Prozessparameter für die Schichtabscheidung.

Coating Process parameter	CrAlN	CrAlVN-1	CrAlVN-2
Total pressure p [mPa]	560	560	560
Argon flow j(Ar) [sccm]	200	200	200
Nitrogen flow j(N_2) [sccm]	Pressure controlled	Pressure controlled	Pressure controlled
Heating power P_H [kW]	8	8	8
Bias voltage U_{Bias} [V]	−100	−100	−100
Average power HPPMS cathodes $P_{HPPMS1/2}$ [kW]	5.0	5.0	5.0
Power of dcMS-1 cathode $P_{dcMS\text{-}1}$ [kW]	4.0	4.0	4.0
Power of dcMS-2 cathode $P_{dcMS\text{-}2}$ [kW]	3.0	2.0	4.5
Power of dcMS-3 cathode $P_{dcMS\text{-}3}$ [kW]	–	2.0	4.5
Power of dcMS-4 cathode $P_{dcMS\text{-}4}$ [kW]	4.0	4.5	4.5

was investigated using cross section images obtained by a scanning electron microscope, ZEISS DSM 982 Gemini, Jena, Germany. The scanning electron microscope was additionally used to determine the chemical contents of chromium, aluminum and vanadium by means of energy dispersive x-ray spectroscopy. A quantification of the nitrogen content with energy dispersive x-ray spectroscopy was omitted. The scanning electron microscopy as well as the energy dispersive x-ray spectroscopy were performed by the Central Facility of Electron Microscopy of the RWTH Aachen University. Nanoindentation measurements were carried out in order to investigate the indentation hardness H_{IT} and the indentation modulus E_{IT} according to DIN EN ISO 14577 as well as the elastic / plastic properties of the coating system. To determine the bulk properties of the coating systems, all nanoindentation measurements were conducted in calotted areas. The calotted areas were prepared by calotte grinding. The maximal material ablation depth within the calotted area was approximately $t_d = 2.0$ µm, *Figure 3*.

For the nanoindentation a Triboindenter TI 959, Bruker Corporation, Billerica, Masschusetts, USA, was used. For the measurements an indentation force of $F = 10$ mN was applied. Subsequently, the evaluation was performed according to an established method. To determine the indentation hardness H_{IT} in accordance to this methode, the indentation force F is divided by the penetrating surface area of the indenter $A_s(h)$. The surface area

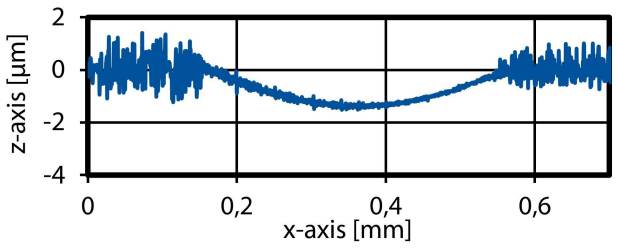

Figure 3. Depth profile of a calotated sample.

Bild 3. Tiefenprofil einer ankalottierten Probe.

$A_s(h)$ is obtained for the Berkovich indenter with half cone- or facet geometry and a pyramidal angle $\alpha_F = 65.03°$ to $A_s(h) = 26.43xh^2$. To determine the indentation modulus E_{IT}, the reduced modulus at indenter contact E_r, the modulus of the indenter E_k, and the Poisson's ratio of the specimen ν_s and the indenter ν_k are required [7]. In order to exclude an impact of substrate used, the indentation depth was limited to approximately 10 % of the coating thickness. The Poisson's ratio was assumed as $\nu = 0.25$. The oxidation stability and phase composition was investigated by means of x-ray diffractometer XRD 3003, GE Energy Germany GmbH, Ratingen, Germany. They were conducted using Cu–Kα radiation at a wavelength of $\lambda = 0.154$ nm, a voltage of $U = 40$ kV, a current of $I = 40$ mA, a diffraction angle of $\omega = 3°$, a step size of $s = 0.05°$ and a step time of $t = 10$ s. The sputter depth profiles of the coating system were measured using x-ray photoelectron spectroscopy. The x-ray photoelectron spectroscopy measurements were conducted by nanoAnalytics GmbH, Münster, Germany.

2.3 Cutting tests

For the cuttings tests, an initial reference process was defined: longitudinal turning of Ti6Al4V with a depth of cut of $a_p = 1.2$ mm, feed rates of $0.12 \text{ mm} \leq f \leq 0.4$ mm, a setting angle of $\kappa_r = 95°$ and cutting velocities of $50 \text{ m/min} \leq v_c \leq 110$ m/min. Tests were conducted using uncoated as well as $((Cr_{61}Al_{17}V_{22})N$ and $(Cr_{51}Al_{12}V_{37})N)$ coated cemented carbide cutting inserts CNGP 120408 of grade HW-K10, Kennametal Deutschland GmbH, Rosbach, Germany, with a corner radius of $r_\varepsilon = 0.8$ mm, an effective rake angle of $\gamma_{eff} = 2°$, an effective clearance angle of $\alpha_{eff} = 6°$ and a cutting edge radius of $r_\beta = 6 + 2$ µm were used, *Figure 4*. The tests were conducted under coolant using emulsion (9 %) consisting of distilled water and cooling lubricant B-Cool 675, Blaser Swisslube AG, Swiss, a Computerized Numerical Control (CNC)-lathe MD5S, Gildemeister Drehmaschinen GmbH, Bielefeld, Germany, equipped with a dynamometer type 9257B, Kistler Instrumente GmbH, Sindelfingen, Germany, for force measurement, Figure 4. As abort criteria, the flank wear land width VB_{max} f = 0.12 mm for finish turning and $VB_{max} = 100$ µm for rough turning as well as a maximum tool life $T = 20$ min were used. The selected time range of $T = 20$ min is based on industrial applications of turning tools for cutting Ti6Al4V. In order to analyze the tool wear precisely and to determine accelerated tool wear in an

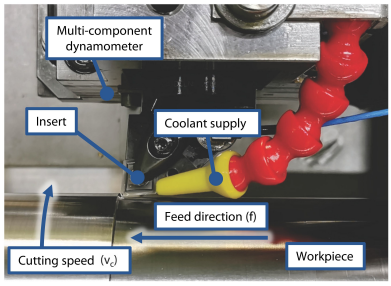

Figure 4. Experimental setup on computerized numerical control (CNC)-lathe Gildemeister MD5S for wear tests using coolant.

Bild 4. Versuchsaufbau auf der computer-numerisch-gesteuerten (CNC)-Drehmaschine Gildemeister MD5S für Verschleißtests mit Kühlschmierstoff.

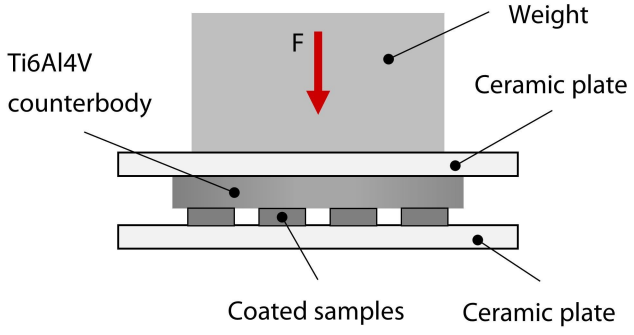

Figure 5. Schematic representation of the experimental sample arrangement for the annealing tests.

Bild 5. Schematische Darstellung des Probenaufbaus während der Auslagerungsversuche.

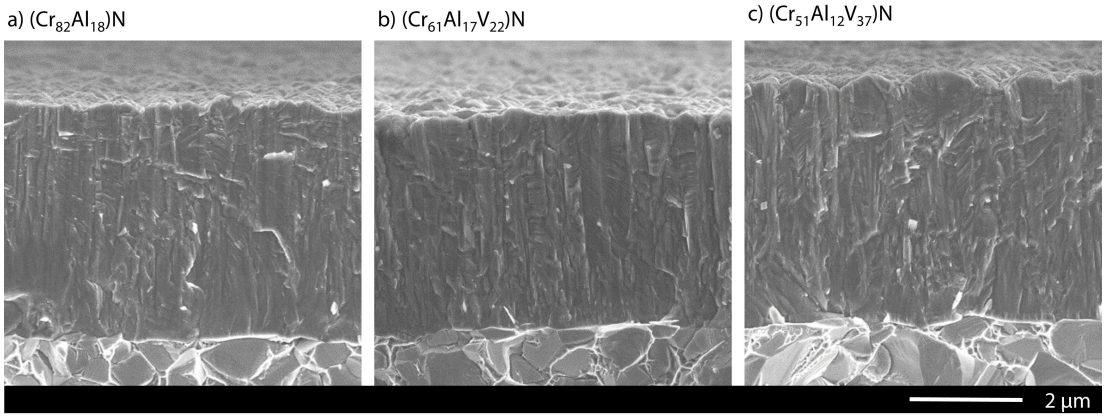

Figure 6. Cross section images of the coating systems $(Cr_{82}Al_{18})N$ (a), $(Cr_{61}Al_{17}V_{22})N$ (b) and $(Cr_{51}Al_{12}V_{37})N$ (c) by scanning electron microscope.

Bild 6. Querbruchaufnahmen der Schichtsysteme $(Cr_{82}Al_{18})N$ (a), $(Cr_{61}Al_{17}V_{22})N$ (b) und $(Cr_{51}Al_{12}V_{37})N$ (c) mittels Rasterelektronenmikroskopie.

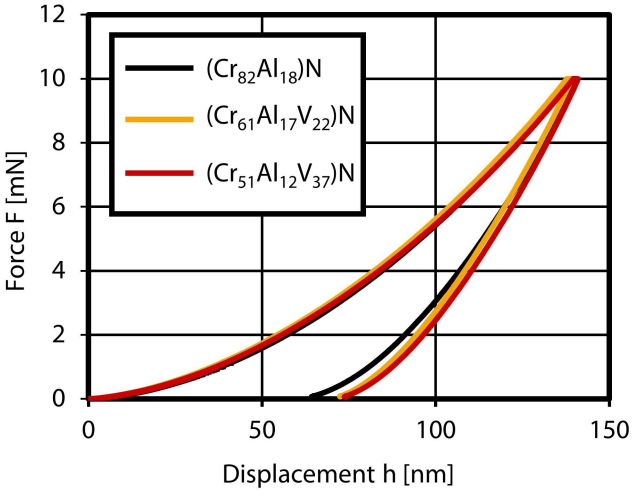

Figure 7. Averaged load displacement curves from nanoindentation.

Bild 7. Gemittelte Kraft-Eindringkurven mittels Nanoindentation.

early stage, the wear occurrences were measured in short intervals within this time range.

2.4 Oxidation behavior

To investigate the fundamental oxidation and diffusion behavior of the different vanadium containing coating systems, heat treatments were carried out under known ambient conditions for $t = 0.5$ h at the temperatures $\vartheta = 600$ °C, $\vartheta = 700$ °C and $\vartheta = 800$ °C with a counterpart made of the titanium alloy Ti6Al4V. This is particularly useful for verifying the ability of the coating to form lubricating oxide phases as well as analyzing the resulting coating properties. Furthermore, the temperatures required for this can be more closely defined by the heat treatments. For this purpose, a cylindrical counterpart made of Ti6Al4V was placed on the coated samples and fixed with a weight of approximately $m = 12$ kg. This chosen weight of $m = 12$ kg is not intended to simulate the stress distribution that occur during turning, but to ensure a uniform contact between the coated surface and the counterpart and to prevent any slipping of the samples during heat treatment. To avoid diffusion between the counterpart and the weight used, a ceramic plate was placed between the two materials, *Figure 5*. For heat treatment, the industrial heat furnace Nabertherm HT 08/17, Nabertherm GmbH, Lilienthal, Germany, was used. For the investigation, the samples were heated up to a temperature of $\vartheta = 500$ °C with a heating rate of approximately $\Delta\vartheta = 16$ °C/min. There, the temperature was maintained for $t = 0.5$ h. In the second step, the temperature was increased to the annealing temperature with a heating rate of approximately $\Delta\vartheta = 13$ °C/min. The annealing temperature was maintained for $t = 0.5$ h. The holding time of $t = 0.5$ h was chosen, to analyze the resulting coating properties after industrial established application times above $t = 20$ min. Subsequently, the fur-

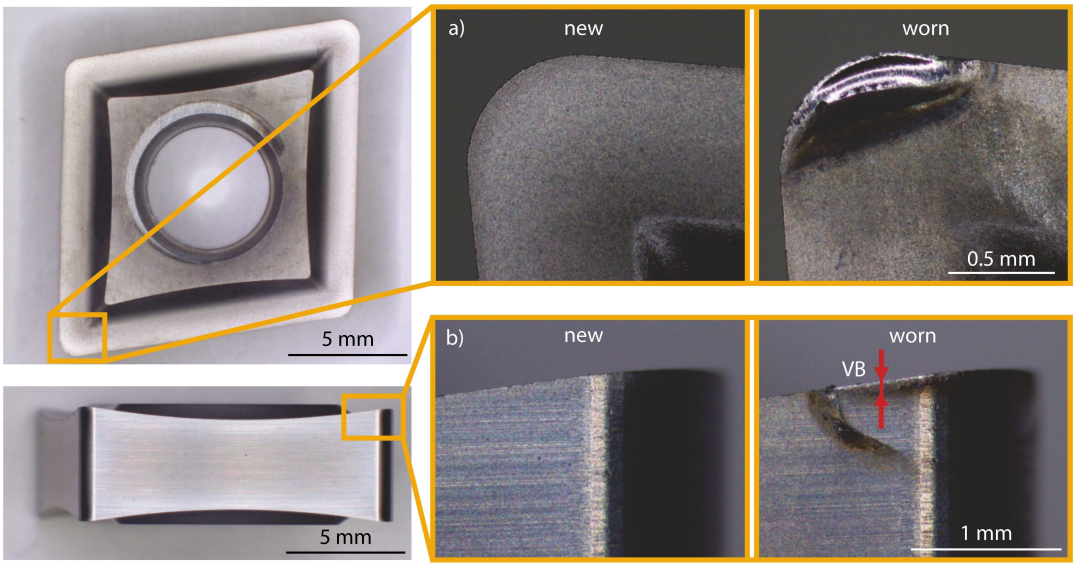

Figure 8. Overview and details of crater wear (a) and flank wear land width VB exemplarily shown at a $(Cr_{61}Al_{17}V_{22})N$ coated insert.

Bild 8. Übersicht und Details des Kolkverschleißes (a) und der Verschleißmarkenbreite VB, exemplarisch dargestellt an einer $(Cr_{61}Al_{17}V_{22})N$-beschichteten Wendeschneidplatte.

nace was switched off, causing the sample to cool down to room temperature.

3 Results

3.1 Coating properties

After deposition, the coating properties of the three different coating systems were analyzed in accordance to the methods mentioned above. The chemical composition of the functional top layer of the three coating systems is different, reasoned by the target configuration and cathode power used, *Table 2*.

The scanning electron microscope cross section images of the three coating systems show a dense fine columnar morphology for the functional top layer in each variant, *Figure 6*. The determined average coating roughness Ra is the same for all variants after deposition. A slight decrease in mean squared roughness Rz is observed with increasing vanadium content of the coating system. The measured coating thickness for $(Cr_{82}Al_{18})N$ and $(Cr_{61}Al_{17}V_{22})N$ is $d_s = 4.0\ \mu m$. Due to the increased cathode power in the process, the coating thickness increases slightly with increasing vanadium content by approximately $\Delta d_s = 0.2\ \mu m$, *Table 3*.

Table 2. Chemical composition after deposition of $(Cr_{82}Al_{18})N$, $(Cr_{61}Al_{17}V_{22})N$ and $(Cr_{51}Al_{12}V_{37})N$ by means of energy dispersive x-ray spectroscopy.

Tabelle 2. Mittels energiedispersiver Röntgenspektroskopie bestimmte chemische Schichtzusammensetzung von $(Cr_{82}Al_{18})N$, $(Cr_{61}Al_{17}V_{22})N$ und $(Cr_{51}Al_{12}V_{37})N$ im Ausgangszustand „as deposited".

Coating system	$(Cr_{82}Al_{18})N$	$(Cr_{61}Al_{17}V_{22})N$	$(Cr_{51}Al_{12}V_{37})N$
Chrome (Cr) [at.-%]	82	61	51
Aluminum (Al) [at.-%]	18	17	12
Vanadium (V) [at.-%]	–	22	37

Nanoindentation measurements were conducted to investigate the indentation hardness H_{IT}, the indentation modulus E_{IT} as well as elastic-plastic deformation behavior of the different physical vapor deposition hard coatings. The resistance against plastic deformation $W_{pl}/(W_{el}+W_{pl})$ was measured with the assumption that an extensive crack formation can be neglected [8].

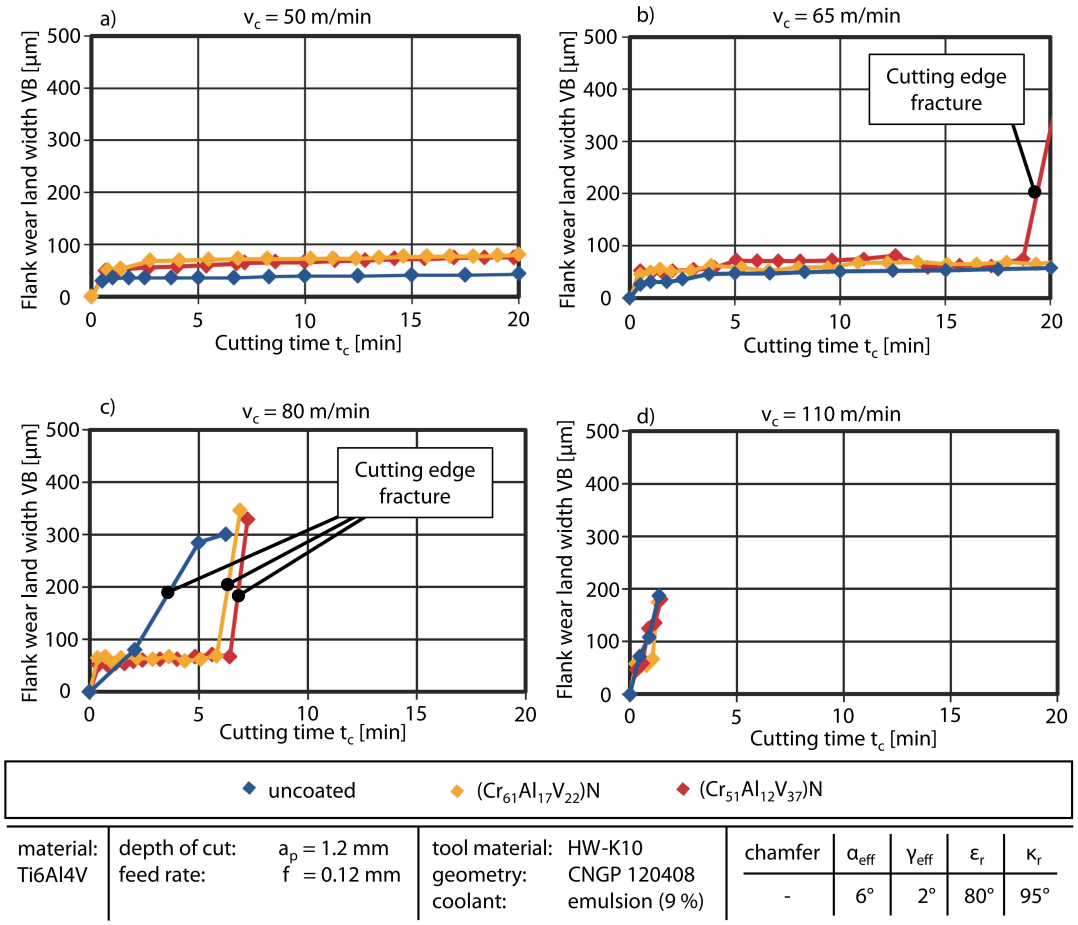

Figure 9. Flank wear land width VB for varied cutting velocities v_c under finishing conditions with constant feed rate f.

Bild 9. Verschleißmarkenbreite VB für unterschiedliche Schnittgeschwindigkeiten v_c unter Schlichtbedingungen mit konstantem Vorschub f.

Table 3. Coating properties of chromium aluminium nitride (CrAlN) and chromium aluminium vanadium nitride (CrAlVN) coatings by means of confocal laser scanning microscopy and nanoindentation depending on the chemical composition after deposition.

Tabelle 3. Mittels konfokalem Lasermikroskop und Nanoindentation bestimmte Schichteigenschaften der Chrom-Aluminium-Nitrid (CrAlN) und Chrom-Aluminium-Vanadium-Nitrid (CrAlVN)-Beschichtungen in Abhängigkeit von Ihrer chemischen Zusammensetzung im Ausgangszustand „as deposited“.

Coating system	$(Cr_{82}Al_{18})N$	$(Cr_{61}Al_{17}V_{22})N$	$(Cr_{51}Al_{12}V_{37})N$
Average coating thickness s [µm]	4.0	4.0	4.2
Average roughness Ra [µm]	0.02	0.02	0.02
Mean squared roughness Rz [µm]	0.17	0.16	0.13
Indentation hardness H_{IT} [GPa]	28.8 ± 4.0	29.6 ± 4.5	28.0 ± 4.2
Indentation modulus E_{IT} [GPa]	294.4 ± 31.2	318.6 ± 36.0	310.5 ± 34.3
Elastic work W_e [pJ]	296.9 ± 25.0	270.2 ± 14.4	269.0 ± 15.4
Plastic work W_p [pJ]	195.6 ± 67.2	228.4 ± 68.1	233.0 ± 61.4
Plasticity index $W_{pl}/(W_{el}+W_{pl})$ [%]	39.7	45.8	46.4

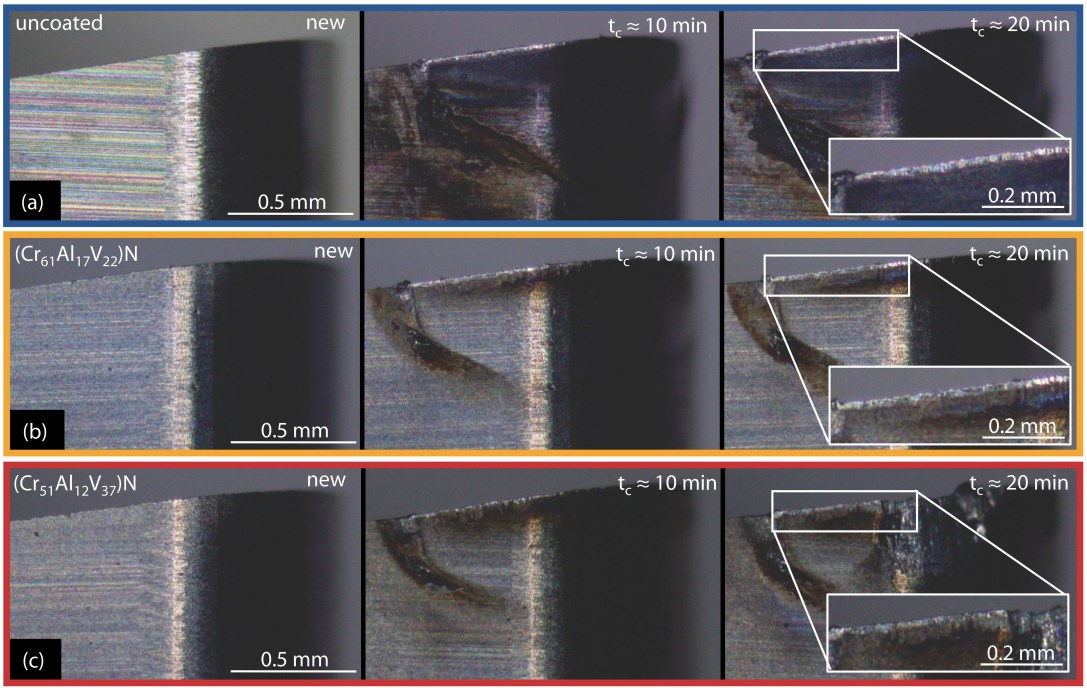

Figure 10. Progress of flank wear land width VB for uncoated, $(Cr_{61}Al_{17}V_{22})N$ and $(Cr_{51}Al_{12}V_{37})N$ coated inserts during finish turning.

Bild 10. Ausbildung der Verschleißmarkenbreite VB für unbeschichtete, $(Cr_{61}Al_{17}V_{22})N$- und $(Cr_{51}Al_{12}V_{37})N$-beschichtete Wendeschneidplatten beim Schlichtdrehen.

The plotted force displacement curves show only a small influence of the chemical coating composition on the plastic deformation behavior. It can be seen, that the displacement h after unloading slightly increases with increasing vanadium content, *Figure 7*. The plasticity index $W_{pl}/(W_{el}+W_{pl})$ increases with increasing vanadium content, Table 3. Therefore, the results of nanoindentation measurements indicate that the coating $(Cr_{82}Al_{18})N$ provides the highest resistance against plastic deformation.

3.2 Cutting tests

Cutting tests were carried out using different machining parameters to investigate the effects of the tool coating on the wear behavior of the inserts. Besides, uncoated cemented carbide inserts were used as reference tools for cutting tests. The cutting parameters used for the wear tests can be assigned to the machining strategies of finish and rough turning, *Table 4*. The flank wear land width VB_{max} is used as tool life criteria. Therefore, in finish turning ($f = 0.12$ mm) the tool is considered as worn at $VB_{max} = 100$ µm. For rough turning ($f = 0.26$ mm, $f = 0.4$ mm) the maximum tool life is reached at $VB_{max} = 300$ µm. The wear

Table 4. Test parameters for the turning experiments.

Tabelle 4. Testparameter für die Drehversuche.

Machining strategy	Depth of cut a_p [mm]	Feed rate f [mm]	Cutting velocity v_c [m/min]	Flank wear land width VB_{max} [µm]
Finish turning	1.2	0.12	50/65/80/110	100
Rough turning	1.2	0.26/0.40	65	300

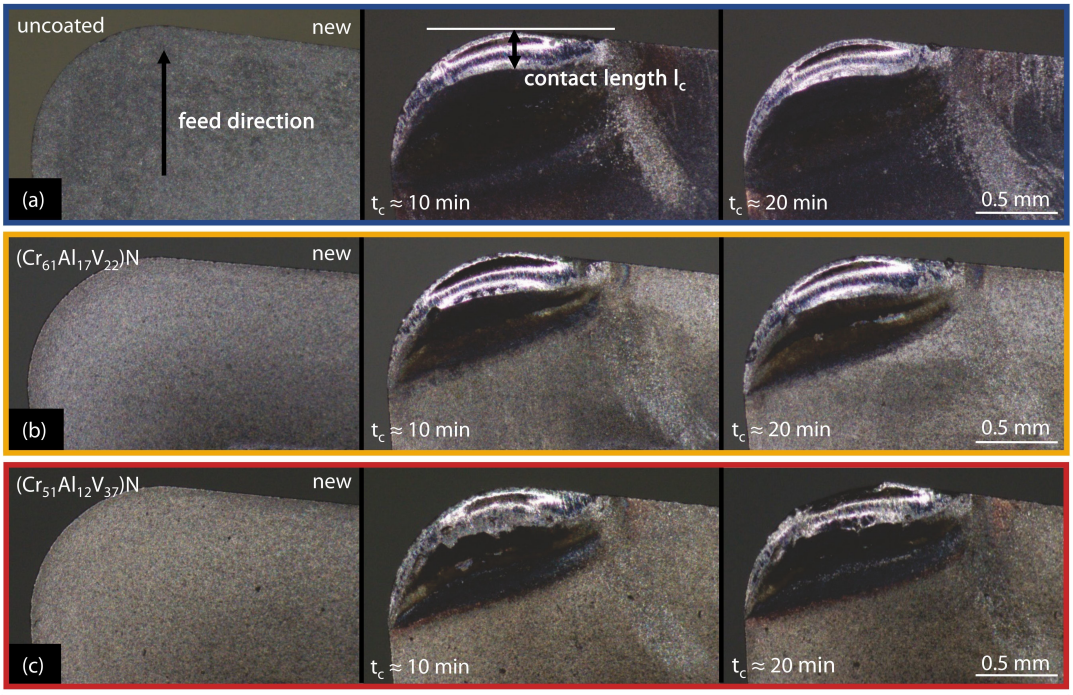

material:	cutting velocity:	v_c = 65 m/min	tool material:	HW-K10
Ti6Al4V	depth of cut:	a_p = 1.2 mm	geometry:	CNGP 120408
	feed rate:	f = 0.12 mm	coolant:	emulsion (9 %)

chamfer	α_{eff}	γ_{eff}	ε_r	κ_r
-	6°	2°	80°	95°

Figure 11. Progress of crater wear and contact length l_c between chip and tool for uncoated, $(Cr_{61}Al_{17}V_{22})N$ and $(Cr_{51}Al_{12}V_{37})N$ coated inserts during finish turning.

Bild 11. Ausbildung des Kolkverschleißes und der Kontaktlänge L_c zwischen Span und Werkzeug für beschichtete, $(Cr_{61}Al_{17}V_{22})N$- und $(Cr_{51}Al_{12}V_{37})N$-beschichtete Wendeschneidplatten beim Schlichtdrehen.

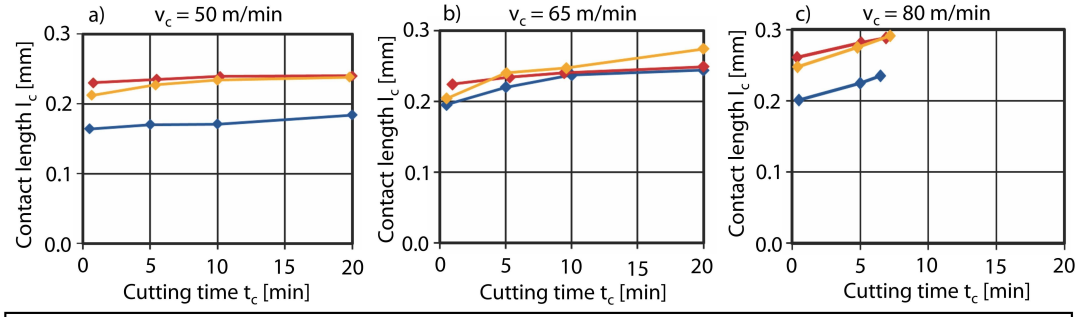

material:	depth of cut:	a_p = 1.2 mm	tool material:	HW-K10
Ti6Al4V	feed rate:	f = 0.12 mm	geometry:	CNGP 120408
			coolant:	emulsion (9 %)

chamfer	α_{eff}	γ_{eff}	ε_r	κ_r
-	6°	2°	80°	95°

Figure 12. Contact length l_c for uncoated, $(Cr_{61}Al_{17}V_{22})N$ and $(Cr_{51}Al_{12}V_{37})N$ coated inserts for varied cutting velocities v_c during finish turning.

Bild 12. Kontaktlänge l_c für unbeschichtete, $(Cr_{61}Al_{17}V_{22})N$- und $(Cr_{51}Al_{12}V_{37})N$-beschichtete Wendeschneidplatten für unterschiedliche Schnittgeschwindigkeiten v_c beim Schlichtdrehen.

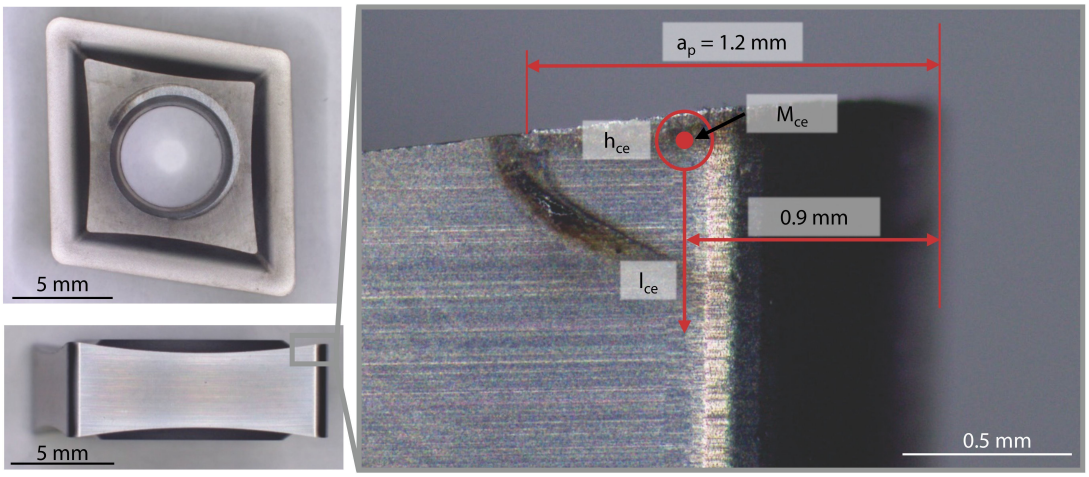

Figure 13. Description of the measurement situation for the measuring of the height profile on the flank surface of the tested inserts.

Bild 13. Beschreibung der Messsituation für die Messung des Höhenprofils auf der Freifläche der getesteten Wendeschneidplatten.

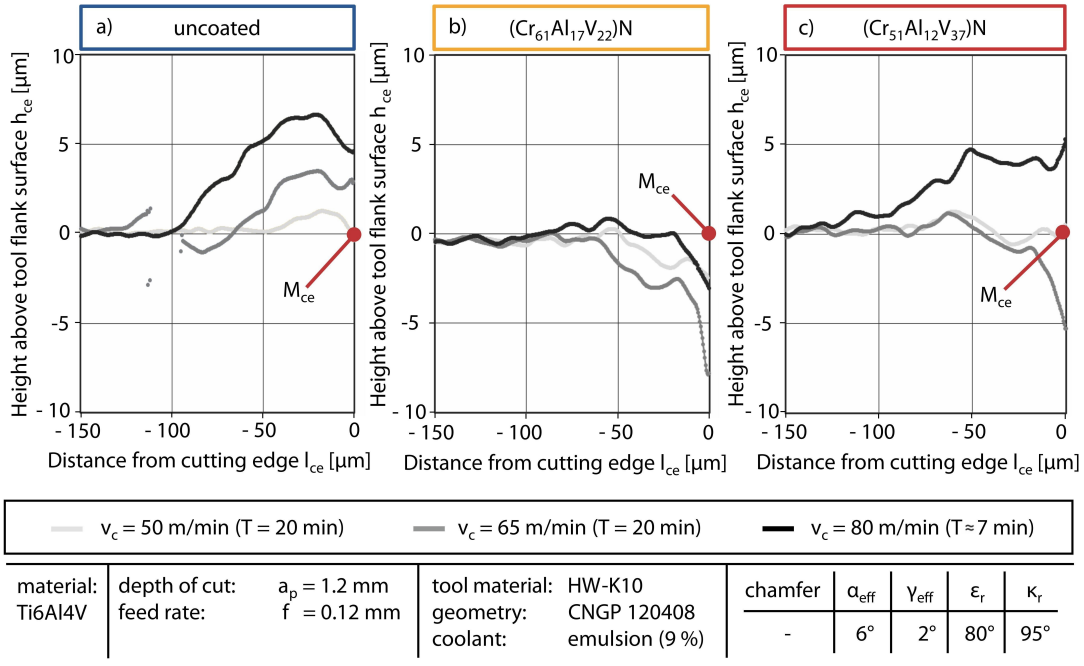

Figure 14. Height above tool flank surface h_{ce} for different cutting velocities v_c for uncoated, $(Cr_{61}Al_{17}V_{22})N$ and $(Cr_{51}Al_{12}V_{37})N$ coated inserts during finish turning at the end of tool life T.

Bild 14. Höhe über der Werkzeugfreifläche H_{CE} für unterschiedliche Schnittgeschwindigkeiten v_c für unbeschichtete, $(Cr_{61}Al_{17}V_{22})N$- und $(Cr_{51}Al_{12}V_{37})N$-beschichtete Wendeschneidplatten beim Schlichtdrehen am Ende der Standzeit T.

which predominantly occurs on the inserts while cutting is crater wear on the rake face, and flank wear on the flank surface, *Figure 8*a, b.

In addition, a maximum tool life of T = 20 min was defined as a further abort criterion for the turning experiments. Significant differences in flank wear land width VB and achievable cutting time t_c can be seen for varied cutting velocities v_c under finishing conditions with a constant feed rate f, *Figure 9*.

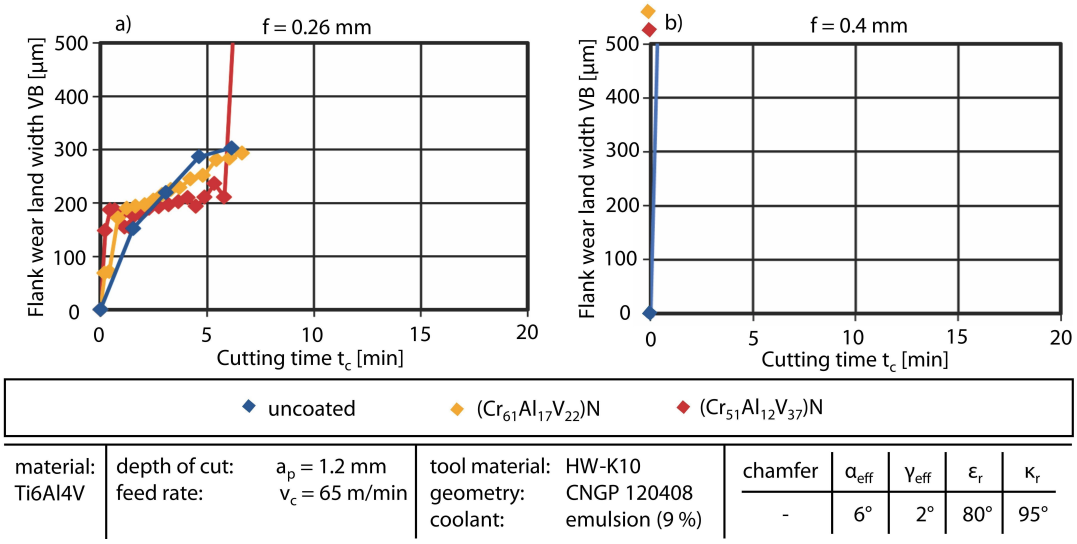

material:	depth of cut:	a_p = 1.2 mm	tool material:	HW-K10
Ti6Al4V	feed rate:	v_c = 65 m/min	geometry:	CNGP 120408
			coolant:	emulsion (9 %)

chamfer	α_{eff}	γ_{eff}	ε_r	κ_r
-	6°	2°	80°	95°

Figure 15. Flank wear land width VB for constant cutting velocity v_c under roughing conditions with varied feed rate f.

Bild 15. Freiflächenverschleiß VB für konstante Schnittgeschwindigkeit v_c unter Schruppbedingungen bei variiertem Vorschub f.

At a cutting velocity of $v_c = 50$ m/min a flank wear land width of VB ≈ 50 µm appears for the inserts with both different coating systems shortly after the start of cutting, Figure 9a. Up to a cutting time of $t_c \approx 2.5$ min, the wear increases to VB ≈ 70 µm. Further on, a small rise to VB ≈ 80 µm can be seen until a cutting time of $t_c = 20$ min. In contrast, the flank wear land width for the uncoated insert increases to VB ≈ 35 µm shortly after the start of cutting, followed by only a slight increase to VB ≈ 45 µm up to a cutting time of $t_c = 20$ min. For a cutting velocity of $v_c = 65$ m/min the flank wear land width VB for the uncoated insert has a similar progression to $v_c = 50$ m/min, Figure 9b. It reaches a value of VB ≈ 30 µm approximately $t_c = 1$ min after the start of cutting and increases slightly to VB ≈ 60 µm until a cutting time of $t_c = 20$ min was reached. The development of the flank wear land width VB for the inserts with the coatings $(Cr_{61}Al_{17}V_{22})N$ and $(Cr_{51}Al_{12}V_{37})N$ is almost similar up to a cutting time of $t_c \approx 18$ min. While the $(Cr_{61}Al_{17}V_{22})N$ coated insert showed a flank wear land width of VB = 75 µm up to a cutting time of $t_c = 20$ min, the cutting edge of the $(Cr_{61}Al_{17}V_{37})N$ coated insert chipped abruptly. A comparison of all three curves shows that the values of the flank wear land width VB between the uncoated and the coated inserts converge at this cutting parameters.

At a cutting velocity of $v_c = 80$ m/min, the $(Cr_{61}Al_{17}V_{22})N$ coated inserts reached a flank wear land width of VB ≈ 65 µm and the $(Cr_{51}Al_{12}V_{37})N$ coated inserts reached a value of VB ≈ 50 µm after a cutting time of $t_c \approx 1$ min, Figure 9c. Further on, for both coated variants the wear increased to VB ≈ 70 µm shortly before a partial cutting edge fracture occurs, after a cutting time of $t_c \approx 7$ min. At this cutting velocity v_c, the flank wear land width VB determined for the uncoated tool exceeds that of the coated tools after a cutting time of $t_c \approx 2$ min with a value of VB ≈ 80 µm. After approximately $t_c \approx 2.5$ min the lifetime criteria of $VB_{max} = 100$ µm was reached for the uncoated tool. This leads to the assumption, that with an increasing cutting velocity v_c, a positive effect of the coatings is more pronounced. In relation to the wear tests at a cutting velocity of $v_c = 80$ m/min, a significant increase in cutting time t_c compared to the uncoated insert can be reached. However, the coated inserts also do not achieve the tool life of T = 20 min, because of a partial cutting edge fracture due to substrate failure.

For a cutting velocity of $v_c = 110$ m/min the maximum cutting time for all tested inserts is below $t_c = 1.5$ min, until the lifetime criteria of $VB_{max} = 100$ µm was reached, Figure 9d. An influence of the different coating systems on the service life of the inserts cannot be detected, whereby it can be assumed that the carbide tool is thermally

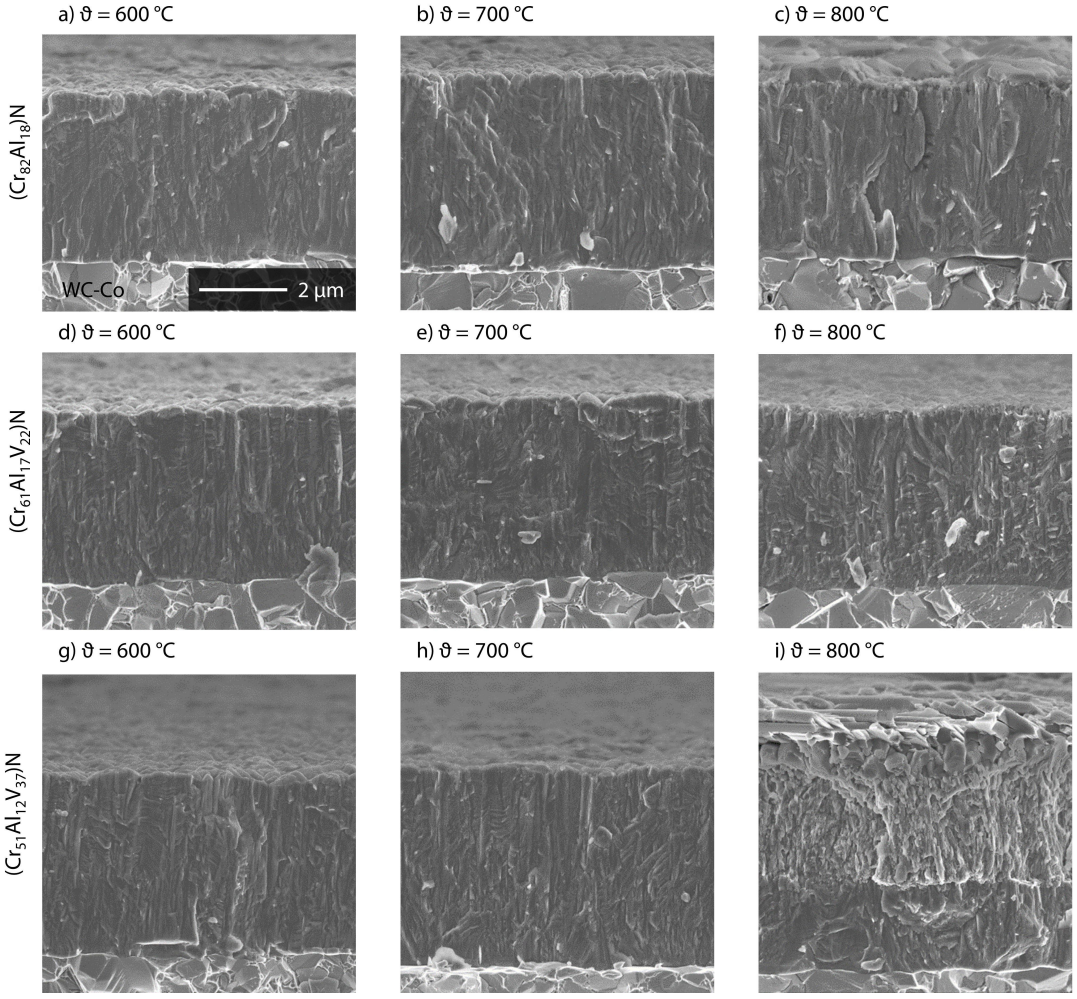

Figure 16. Scanning electron microscope cross sections of $(C_{82}Al_{18})N$, $(Cr_{61}Al_{17}V_{22})N$ and of $(Cr_{51}Al_{12}V_{37})N$ after heat treatment in ambient atmosphere for t = 0,5 h at $\vartheta = 600$ °C, $\vartheta = 700$ °C and $\vartheta = 800$ °C in contact with a Ti6Al4V counterpart.

Bild 16. Rasterelektronenmikroskopische Querbruchaufnahmen der Schichtsysteme $(Cr_{82}Al_{18})N$ (a), $(Cr_{61}Al_{17}V_{22})N$ (b) und $(Cr_{51}Al_{12}V_{37})N$ (c) nach Auslagerung an Umgebungsatmosphäre für t = 0,5 h bei $\vartheta = 600$ °C, $\vartheta = 700$ °C und $\vartheta = 800$ °C mit TiAl6V4 Gegenkörper.

and mechanically overloaded at this cutting velocity in combination with the selected depth of cut $a_p = 1.2$ mm and the feed rate of f = 0.12 mm.

Based on the present wear tests, advantages of the coated inserts at higher cutting velocities can be seen, in particular for a cutting velocity of $v_c = 80$ m/min. This advantage of self-lubricating chromium aluminium vanadium nitride (CrAlVN) coatings at higher cutting velocities v_c forms the basis for more economical machining of the titanium alloy Ti6Al4V through increased metal removal rates. The following comparison of the wear pattern of the uncoated and the $(Cr_{61}Al_{17}V_{22})N$ and $(Cr_{51}Al_{12}V_{37})N$ coated inserts during finish turning shows differences in wear behavior at a cutting velocity of $v_c = 65$ m/min and a feed rate of f = 0.12 mm, *Figure 10*.

Comparing the flank wear of both coated tools, it is apparent that there are less reflections visible at the cutting edge of the insert coated with $(Cr_{51}Al_{12}V_{37})N$. This indicates a reduced substrate exposure relative to the insert with the $(Cr_{61}Al_{17}V_{22})N$ coating. Accordingly the $(Cr_{51}Al_{12}V_{37})N$ coating has a higher resistance to abrasive wear, Figure 10b, c. In case of the uncoated insert, the area where the substrate material shows visible signs of wear is comparable to the $(Cr_{61}Al_{17}V_{22})N$ coated insert and larger than for the $(Cr_{51}Al_{12}V_{37})N$ coated insert, Figure 10a.

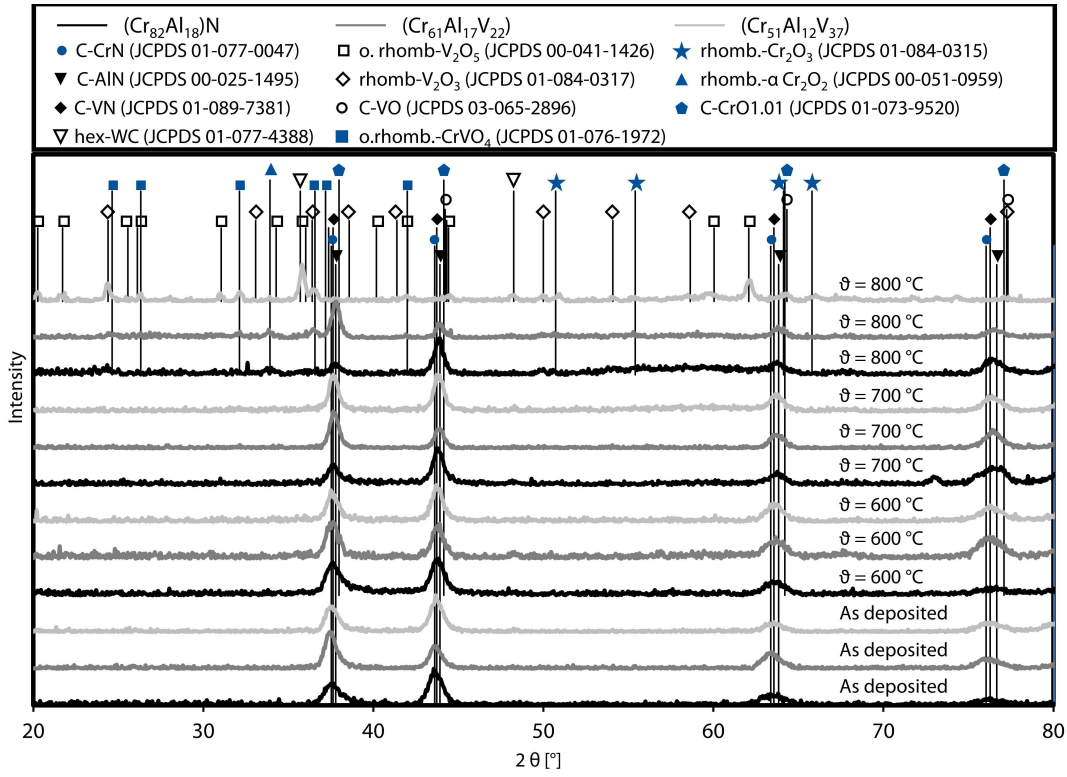

Figure 17. X-ray diffractometric measurements of $(Cr_{82}Al_{18})N$, $(Cr_{61}Al_{17}V_{22})N$ and $(Cr_{51}Al_{12}V_{37})N$ in the initial state "as deposited" and after annealing for t = 0.5 h at ϑ = 600 °C, ϑ = 700 °C and ϑ = 800 °C in ambient atmosphere, with an Ti6Al4V counterpart.

Bild 17. Röntgendiffraktometrische Analysen der Schichtsysteme $(Cr_{82}Al_{18})N$ (a), $(Cr_{61}Al_{17}V_{22})N$ (b) und $(Cr_{51}Al_{12}V_{37})N$ (c) im Ausgangszustand „as deposited" und nach Auslagerung an Umgebungsatmosphäre für t = 0,5 h bei ϑ = 600 °C, ϑ = 700 °C und ϑ = 800 °C mit TiAl6V4 Gegenkörper.

In general, consistent wear with minor chipping over the cutting edge area can be observed for all test variants. Additionally, over the tool life T = 20 min, the coated inserts show no coating delamination or crack formation. Only the $(Cr_{51}Al_{12}V_{37})N$ coated insert shows a partial cutting edge fracture at T = 20 min, Figure 10c. Furthermore, an almost constant formation of notch wear at the major cutting edge for all tested inserts is found. This applies to all cutting conditions.

When examining the wear progress on the rake face, it can be seen that after cutting, crater wear is clearly visible for all tested variants, *Figure 11*.

After a cutting time of t_c = 10 min, the crater wear on the $(Cr_{61}Al_{17}V_{22})N$ coated insert is much more pronounced than for the $(Cr_{51}Al_{12}V_{37})N$ coated insert. These observations indicate a different wear behavior depending on the stoichiometry of the coated inserts. When examining the contact lengths l_c between chip and insert, similar characteristics can be observed for the $(Cr_{61}Al_{17}V_{22})N$ and the $(Cr_{51}Al_{12}V_{37})N$ coated insert, *Figure 12*. For cutting velocities of v_c = 50 m/min and v_c = 65 m/min the contact length for both coated tools is rising to $l_c \approx 0.24$ mm until a cutting time of t_c = 5 min and remains almost constant until T = 20 min. A slight deviation in this behavior can be seen for the $(Cr_{61}Al_{17}V_{22})N$ coated insert at a cutting velocity of v_c = 65 m/min, since the contact length increases to a value of $l_c \approx 0.28$ mm, Figure 12a, b.

At a cutting velocity of v_c = 80 m/min the tool life criterion of a flank wear land width VB_{max} = 100 µm is already reached after a cutting time of $t_c \approx 7$ min. This is due to the faster wear progress at v_c = 80 m/min, which leads to a steady increase in contact length l_c, Figures 9, 12c. When comparing the contact lengths of the uncoated and the coated inserts, a considerably lower contact length l_c can be seen for the uncoated insert at

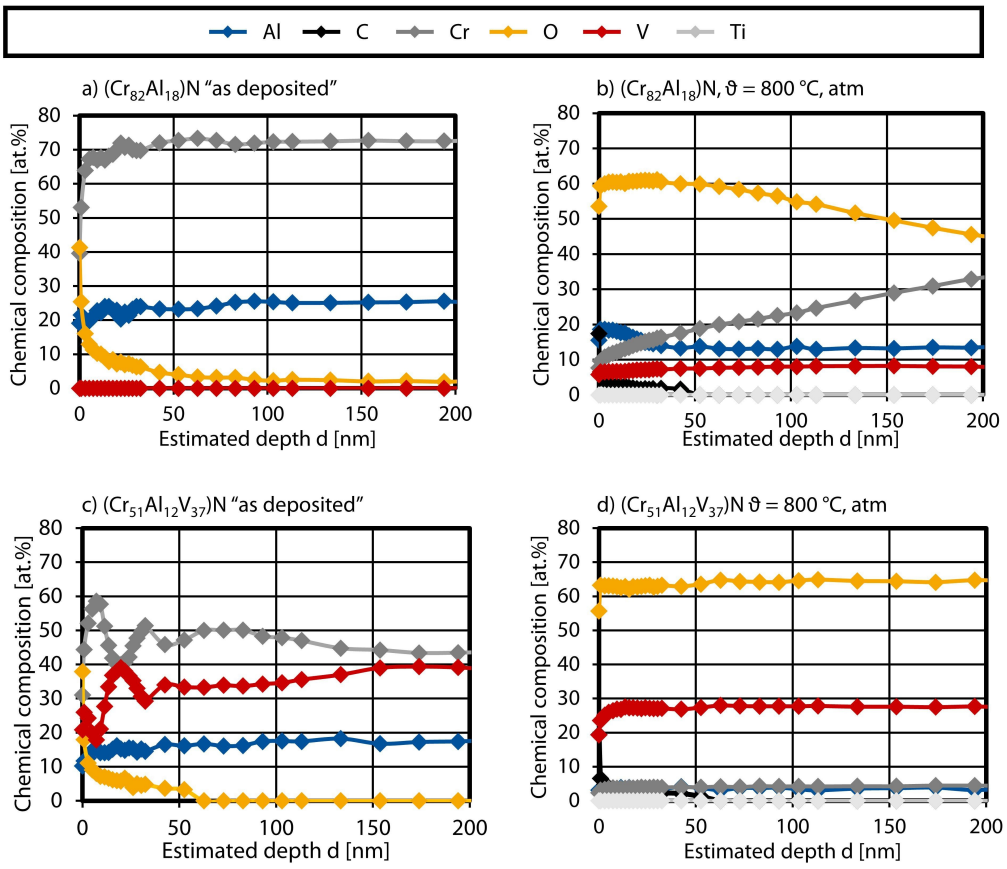

Figure 18. X-ray photoelectron spectroscopy sputter depth profiles of $(Cr_{82}Al_{18})N$ and $(Cr_{51}Al_{12}V_{37})N$ in the initial state "as deposited" and after annealing for t = 0.5 h at ϑ = 800 °C in ambient atmosphere, with an Ti6Al4V counterpart.

Bild 18. Röntgenphotoelektronenspektroskopische Sputtertiefenprofile von $(Cr_{82}Al_{18})N$ und $(Cr_{51}Al_{12}V_{37})N$ im Ausgangszustand „as deposited" und nach der Auslagerung für τ = 0,5 h bei ϑ = 800 °C in Umgebungsatmosphäre, mit einem TiAL6V4 Gegenkörper.

$v_c = 50$ m/min and $v_c = 80$ m/min. At $v_c = 65$ m/min, the contact lengths l_c of the uncoated and coated inserts are almost the same. Similar to the investigation of the flank wear land width VB, an increasing tendency of the contact length l_c for the uncoated insert can be seen for increasing cutting velocities v_c, especially at $v_c = 50$ m/min and $v_c = 65$ m/min, Figure 9.

As for the coated and uncoated inserts almost identical forces were measured, higher contact lengths lead to reduced specific mechanical and thermal stresses at the cutting edge. This prevents plastic deformation of the cutting edge [9]. In order to investigate the influence of the coating systems $(Cr_{61}Al_{17}V_{22})N$ and $(Cr_{51}Al_{12}V_{37})N$ on plastic deformations, the height profiles of the flank surface of the inserts were measured using an Alicona InfiniteFocus G4, Alicona Imaging GmbH, Graz, Austria. The height profiles were determined from the point M_{ce} along the path of l_{ce}, *Figure 13*. The point M_{ce} is located at 75 % of the depth of cut a_p, id est 0.9 mm. The measuring distance starting from the point M_{ce} is $l_{ce} = 150$ µm.

When comparing the plastic deformation of the coated and the uncoated inserts distinct differences are obvious. In case of the uncoated insert pronounced plastic deformations already occur at a cutting velocity of $v_c = 50$ m/min. With increasing cutting velocities v_c these deformations become more intense up to a height above flank surface of $h_{ce} \approx 7$ µm at $v_c = 80$ m/min, *Figure 14*a. In contrast, the determined height profiles of the flank surfaces for both coated inserts show no significant plastic deformations at cutting velocities of $v_c = 50$ m/min and $v_c = 65$ m/min, Figure 14b, c. The curves have a negative progression towards the

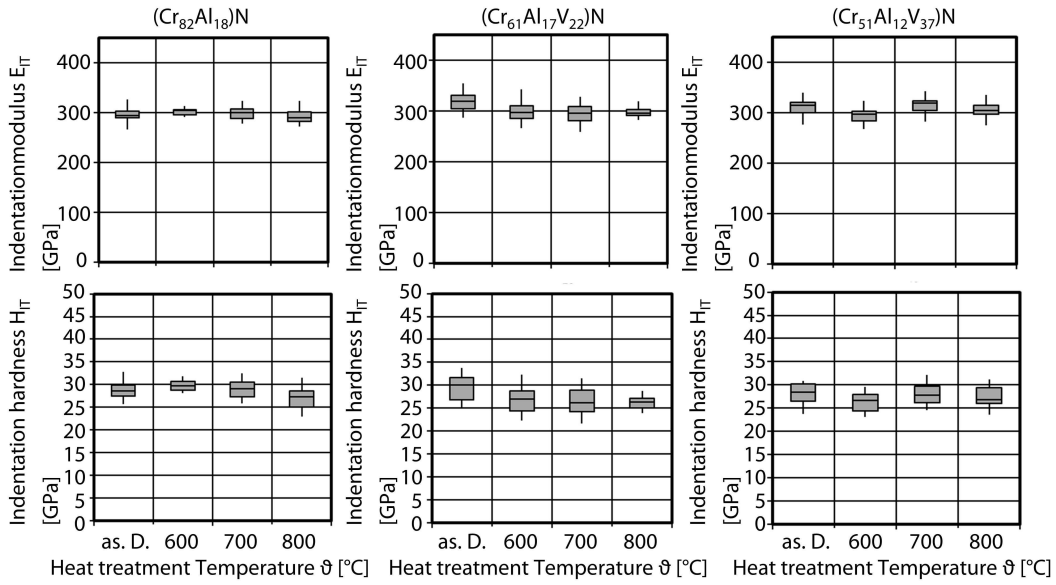

Figure 19. Indentation hardness H_{IT}, indentation modulus E_{IT} of $(Cr_{82}Al_{18})N$, $(Cr_{61}Al_{17}V_{22})N$, $(Cr_{51}Al_{12}V_{37})N$ in the initial state "as deposited" and after heat treatment for t = 0.5 h at ϑ = 600 °C, ϑ = 700 °C and ϑ = 800 °C in ambient atmosphere, with an Ti6Al4V counterpart.

Bild 19. Eindringhärte H_{IT} und Eindringmodul E_{IT} von $(Cr_{82}Al_{18})N$, $(Cr_{61}Al_{17}V_{22})N$, $(Cr_{51}Al_{12}V_{37})N$ im Ausgangszustand „as deposited" und nach Auslagerung für τ = 0,5 h bei ϑ = 600 °C, ϑ = 700 °C und ϑ = 800 °C in Umgebungsatmosphäre, mit einem TIAL6V4 Gegenkörper.

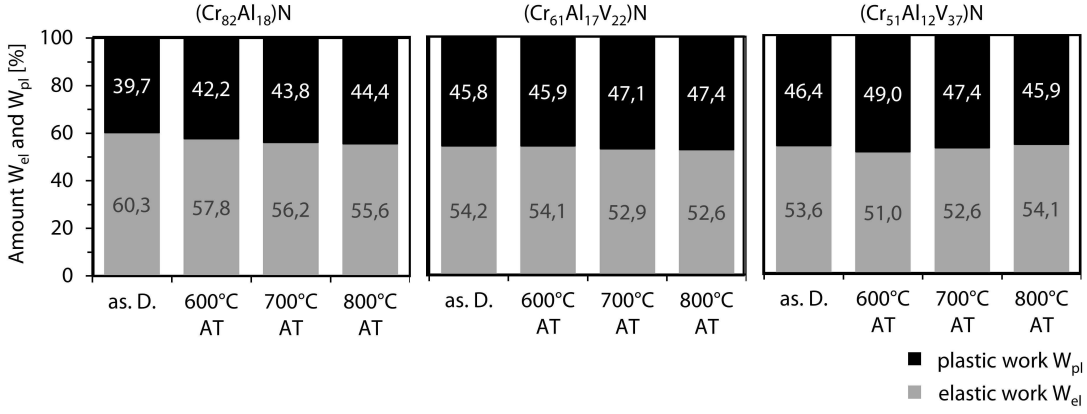

Figure 20. Plastic Work W_{pl} and elastic Work W_{el} of $(Cr_{82}Al_{18})N$, $(Cr_{61}Al_{17}V_{22})N$ and $(Cr_{51}Al_{12}V_{37})N$ in the "as deposited" state and after heat treatment for t = 0.5 h at ϑ = 600 °C, ϑ = 700 °C and ϑ = 800 °C in ambient atmosphere, with a TI6Al4V counterpart.

Bild 20. Plastische Arbeit W_{PL} und elastische Arbeit W_{EL} von den Schichtsystemen $(Cr_{82}Al_{18})N$, $(Cr_{61}Al_{17}V_{22})N$, $(Cr_{51}Al_{12}V_{37})N$ im Ausgangszustand „as deposited" und nach Auslagerung für τ = 0,5 h bei ϑ = 600 °C, ϑ = 700 °C und ϑ = 800 °C in Umgebungsatmosphäre, mit einem TIAL6V4 Gegenkörper.

cutting edge for the height above tool flank surface h_{ce}, corresponding to the abrasive wear on the flank surface, Figure 9. However, the abrasive flank wear marks are not smooth oriented in the effective direction but are characterized by micro chipping of the coated cutting edges extending to a distance of about l_{ce} = 50 µm from the cutting edge. At a cutting velocity of v_c = 80 m/min for the $(Cr_{51}Al_{12}V_{37})N$ coated insert a plastic deformation similar to that of the uncoated insert is stated. This can be ex-

plained by the partial cutting edge fracture which subsequently leads to a rising thermomechanical loading of the insert substrate, Figure 10c.

Considering roughing conditions with various increased feed rates $f = 0.26$ mm and $f = 0.4$ mm at a moderate constant cutting velocity of $v_c = 65$ m/min results in a significantly increased wear progress on the flank surface, *Figure 15*. Based on the predefined tool life criterion of $VB_{max} = 300$ µm for rough turning, all tested inserts reached a tool life of $T = 6$ min for the feed rate of $f = 0.26$ mm, Figure 15a. When the feed rate f was increased to $f = 0.4$ mm, massive cutting edge fracture due to catastrophic substrate failure occurred in all cases, resulting from thermomechanical overload, Figure 15b.

3.3 Oxidation behavior

The oxidation behavior of $(Cr_{82}Al_{18})N$, $(Cr_{61}Al_{17}V_{22})N$ and $(Cr_{51}Al_{12}V_{37})N$ was analyzed by annealing in ambient atmosphere for $t = 0.5$ h at $\vartheta = 600$ °C, $\vartheta = 700$ °C and $\vartheta = 800$ °C in contact with an Ti6Al4V counterpart. Scanning electron microscope images indicates changes in the coating morphology structure after heat treatments, *Figure 16*. In comparison to the initial state "as deposited", the morphology of all three coating systems did not change significantly after heat treatment at $\vartheta = 600$ °C, Figure 16a, d, g. After heat treatment at $\vartheta = 700$ °C a slight coarsening of the columns in $(Cr_{82}Al_{18})N$ is visible, Figure 16b. In contrast to that, the morphology of both vanadium containing coating systems show still no obvious changes, Figure 16e, h.

After annealing at $\vartheta = 800$ °C, all three coatings exhibit a change in morphology, Figure 16c, f, i. In $(Cr_{82}Al_{18})N$ the coarsening of the columns increases and the formation of vaulted structures on the surface is visible, Figure 16c. $(Cr_{61}Al_{17}V_{22})N$ shows a change in the orientation of the columns, with the result that the structure appears more disordered, Figure 16f. However, the greatest changes after annealing at $\vartheta = 800$ °C can be observed for $(Cr_{51}Al_{12}V_{37})N$, Figure 16i. The coating thickness increases by approximately $s = 2$ µm compared to the initial state, due to the formation of an oxidic reaction layer on the surface. Additionally, the appearance of the morphology indicates the formation of three different layers, Figure 16i. The bottom layer in the morphology seems to be almost unchanged. This is followed by a transition layer in the middle. The third, near-surface layer shows elongated structures, which seems to be molten during annealing at $\vartheta = 800$ °C. The changes might result from diffusion and oxidation processes of vanadium and the formation of oxide phases with a comparatively low melting point, such as vanadium (V)-oxide (V_2O_5).

X-ray diffractometric measurements of the coating systems $(Cr_{82}Al_{18})N$, $(Cr_{61}Al_{17}V_{22})N$ and $(Cr_{51}Al_{12}V_{37})N$ were carried out in the "as deposited" state and after annealing in ambient atmosphere for $t = 0.5$ h at $\vartheta = 600$ °C, $\vartheta = 700$ °C and $\vartheta = 800$ °C, *Figure 17*. The x-ray diffractometric measurements were conducted in order to investigate the oxidation behavior of the coating systems. After annealing at $\vartheta = 600$ °C, chromium oxides peaks can be detected beside the peaks for cubic phases aluminum nitride (AlN), chromium nitride (CrN) and vanadium nitride (VN). Up to a temperature of $\vartheta = 800$ °C no additional oxide peaks are detected. From a temperature of $\vartheta = 800$ °C, several oxide peaks are detected, most of them for the coating system $(Cr_{51}Al_{12}V_{37})N$. The oxide peaks can be assigned to the oxides vanadium(III)-oxide (V_2O_3), vanadium(V)-oxide (V_2O_5), vanadium(II)-oxide (VO), chromium-vanadium (IV)-oxide ($CrVO_4$), chromium(II)-oxide (Cr_2O_2), chromium(III)-oxide (Cr_2O_3).

Additionally, the oxidation behavior of $(Cr_{82}Al_{18})N$ and $(Cr_{51}Al_{12}V_{37})N$ was investigated by x-ray photoelectron spectroscopy. For this purpose, measurements were carried out in the "as deposited" state and after annealing at $\vartheta = 800$ °C for $t = 0.5$ h in ambient atmosphere with a Ti6Al4V counterpart. Compared to the "as deposited" state, *Figure 18*a, the chemical composition of the $(Cr_{82}Al_{18})N$ coating exhibits a strong increase in oxygen after annealing, Figure 18b. Additionally, a shift of the aluminum to chromium ratio can be seen after the heat treatment. Up to a depth of approximately $d = 20$ nm, the chromium content is lower compared to the aluminum content. Furthermore, an additional amount of vanadium of approximately $x(V) = 8$ at% is detectable after heat treatment at $\vartheta = 800$ °C for $t = 0.5$ h in ambient atmosphere with an Ti6Al4V counterpart. The appearance of vanadium is attributed to diffusion

processes between the coating system and the Ti6Al4V. An analysis of the counterparts is currently being carried out and will be part of a later publication. Compared to the other chemical elements of the coating system $(Cr_{51}Al_{12}V_{37})N$ a strong increase of the oxygen and vanadium content in the surface near area up to the analyzed depth of $d = 200$ nm is measurable after the heat treatment. Due to the comparatively high vanadium content of the coating system, the increase of vanadium in the surface zone is attributed to diffusion processes within the coating system.

Indentation hardness H_{IT} and Indentation modulus E_{IT} were measured, in the "as deposited" state and after heat treatment for $t = 0.5$ h at $\vartheta = 600$ °C, $\vartheta = 700$ °C and $\vartheta = 800$ °C, *Figure 19*. Within the standard deviation, no significant changes of the indentation hardness H_{IT} and the indentation modulus E_{IT} can be observed for all three coating systems after heat treatment of $\vartheta = 600$ °C, $\vartheta = 700$ °C and $\vartheta = 800$ °C. This is attributed to the fact that the indentation hardness and the indentation modulus were determined within a calotted area and therefore reflect the bulk properties of the coating system. As the scanning electron microscope images, also indicate, the bulk material is almost unaffected by the near surface oxidation, Figure 16. In particular, this result is rather unsuspected for the coating $(Cr_{51}Al_{12}V_{37})N$, since it exhibits strong oxidation within almost the whole cross section area, Figure 16i. Reasons for this are currently part of the investigations.

The resistance against plastic deformation $W_{pl}/(W_{el} + W_{pl})$ was measured with the assumption, that an extensive crack formation can be neglected. For the coating systems $(Cr_{82}Al_{18})N$ and $(Cr_{61}Al_{17}V_{22})N$ a slight increase of $W_{pl}/(W_{el} + W_{pl})$ can be observed after annealing at $\vartheta = 600$ °C, $\vartheta = 700$ °C and $\vartheta = 800$ °C, *Figure 20*. The coating system $(Cr_{51}Al_{12}V_{37})N$ also shows a slight increase of $W_{pl}/(W_{el} + W_{pl})$ after annealing at $\vartheta = 600$ °C. However, after annealing at $\vartheta = 700$ °C and $\vartheta = 800$ °C, $W_{pl}/(W_{el} + W_{pl})$ drop again. It reaches the lowest value compared to the "as deposited" state after annealing at $\vartheta = 800$ °C with $W_{pl} = 45.9$ %. Overall $(Cr_{82}Al_{18})N$ shows the best elastic-plastic properties, both in the initial state as well as after annealing processes.

4 Conclusion

In order to increase the economic efficiency while turning titanium alloy Ti6Al4V, the use of self-lubricating coating systems based on the functional principle of lubricating oxide phases is a suitable approach. Overall, the following findings are highlighted:

- Carbide inserts were successfully coated with the self-lubricating coating systems $(Cr_{61}Al_{17}V_{22})N$ and $(Cr_{51}Al_{12}V_{37})N$.
- Cutting tests on a Computerized Numerical Control (CNC)-lathe with various finishing and roughing parameters indicate a range of parameters in which the machining of Ti6Al4V basically works.
- Finish turning at $v_c = 80$ m/min and $f = 0.12$ mm shows a clear tool life advantage and therefore an increased economic efficiency of the coated cutting tools, compared to the uncoated reference can be achieved.
- The $(Cr_{51}Al_{12}V_{37})N$ coated carbide inserts show a higher resistance to abrasive wear on the flank face compared to the $(Cr_{61}Al_{17}V_{22})N$ coated and uncoated inserts.
- The contact length of the formed chips on the rake face of the coated inserts are higher whereby the thermomechanical loads are better distributed over the cutting edge of the insert.
- After annealing in ambient atmosphere, especially at $\vartheta = 800$ °C, several lubricating oxide phases are found in the coating system using x-ray diffractometric measurements.

Acknowledgement

The author gratefully acknowledge the financial support of the German Research Foundation, Deutsche Forschungsgemeinschaft (DFG) within the research project BO 1979/69-1/HI 843/10-1. Open access funding enabled and organized by Projekt DEAL.

5 References

[1] F. Klocke, *Zerspanung mit geometrisch bestimmter Schneide*, Springer Vieweg, Berlin **2018**.
[2] B.M. Kramer, D. Viens, S. Chin, *CIRP Ann.* **1993**, *42*, 111.
[3] G.G. Ye, S.F. Xue, X.H. Tong, L.H. Dai, *AM + R* **2011**, *337*, 387.
[4] H. Czichos, K.-H. Habig, *Tribologie-Handbuch*, Springer Vieweg, Wiesbaden **2015**.
[5] A. Magnéli, *Acta Cryst* **1953**, *6*, 495.
[6] K. Bobzin, T. Brögelmann, G. Grundmeier, T. de los Arcos, M. Wiesing, N.C. Kruppe, *Surf. Coat. Technol.* **2016**, *308*, 394.
[7] W.C. Oliver, G.M. Pharr, *J. Mater. Res.* **1992**, *7*, 1564.
[8] K. Bobzin, T. Brögelmann, R.H. Brugnara, M. Arghavani, T.-S. Yang, Y.-Y. Chang, S.-Y Chang, *Surf. Coat. Technol.* **2015**, *284*, 310.
[9] P.A. Dahlman, *J. Eng.Manuf.* **2002**, *216*, 467.

Received in final form: July 22nd 2021

